Nonequilibrium Processes in Supersonic Jets of N_2, H_2, and $N_2 + H_2$ Mixtures: (I) Zone of Silence

A. Ramos,* G. Tejeda, J. M. Fernández, and S. Montero

Laboratory of Molecular Fluid Dynamics, Instituto de Estructura de la Materia, CSIC, Serrano 121, 28006 Madrid, Spain

Received: February 24, 2009; Revised Manuscript Received: June 12, 2009

Number density and rotational temperature in the zone of silence of supersonic jets of N_2, H_2, and their mixtures $N_2 + 2H_2$ and $2N_2 + H_2$, at $p_0 = 1$ bar and $T_0 = 295$ K, have been measured by Raman spectroscopy. Translational temperature in the jets has been derived from the experimental data assuming isentropic flow. The density along the jet axis decays at a rate depending on the composition of the expanded gas, which can be explained by the variation of its effective heat capacity ratio. Measurements across the jet axis do not support numerical off-axis density modeling from the literature. A strong nonequilibrium between the rotational degrees of freedom of both species is observed, even between the two spin species ortho-H_2 and para-H_2. From the corresponding rotational temperature data, a relationship between rotational cross sections for the inelastic collisions of the different species is established. In the expansions of the mixtures, an enrichment of N_2 is measured on the axis, which is compared with the predictions from the theory of diffusive separation in jets.

Introduction

Supersonic flow of gas mixtures is present in a wide range of scientific and technical problems, including the study of comets, aeronomy and propulsion in connection with planetary atmospheres, species separation, vacuum technology, and materials science, among others. The kinetic theory of gas mixtures is quite complicated,[1,2] even with the absence of chemical reactions, while the direct simulation Monte Carlo (DSMC) procedure is computationally expensive. Thus, the interpretation of supersonic jets of gas mixtures is progressing slowly, a fact aggravated by the shortage of accurate experimental data.

The supersonic expansion of mixed molecular gases is accompanied by several simultaneous nonequilibrium processes. In the zone of silence of the jet,[3] these include the breakdown of local equilibrium between the different degrees of freedom and diffusive separation, as well as velocity and temperature slip effects between species. If the molecular masses and collision cross sections of the species in the mixture are quite different, the mentioned effects are important and difficult to predict precisely on the sole basis of the current theoretical and numerical methods.

The nonequilibrium between degrees of freedom in the zone of silence of pure and mixed molecular gas jets has been employed to derive information about the state-to-state rate coefficients for inelastic collisions. These coefficients quantify the exchange of translational−rotational energy due to the molecular collisions.[4−7] Such a detailed study of the collisional processes is of interest because they shape a wide range of transport phenomena like thermal conductivity, shear and volume viscosity, diffusion, and broadening of spectral lines, among others.[8]

Species separation in the expansion of a binary mixture is due to a barodiffusive effect. This phenomenon, known since the 1950s, produces an enrichment of the heavy species in the paraxial core of the jet. It was initially attributed to the intrusive effect of the gas sampling probe,[9] but later theoretical developments confirmed the diffusive separation of the mixture.[10] Since then, it has been employed to explain the experimental separation of binary mixtures.[11−13] The spatial and kinetic energy distribution of species within the jet, due to this effect as well as to aerodynamic focusing[14] or velocity slip,[15] are of particular interest in film deposition technology and in the generation of nanoparticles.[16]

In the present work, we have studied the $N_2 + H_2$ system, focusing our attention on the nonequilibrium between degrees of freedom and on the diffusive separation of species. The $N_2 + H_2$ mixture is of technological interest since N_2 and H_2 are the main momentum carriers, jointly with NH_3, of the thrust in a hydrazine (N_2H_4) resistojet.[17] DSMC modeling of this flow field is quite sensitive to the molecular interaction, and so, the validation of DSMC solutions requires detailed experimental measurements of the flow quantities.[18] Besides, there is an intrinsic interest in this system because N_2 and H_2 have very different molecular properties. Their disparity of mass and intermolecular potential energy lead, in the supersonic expansions, to a strong nonequilibrium between the translational and the rotational temperatures of N_2 and H_2, whose two spin species, ortho and para-hydrogen, are also out of equilibrium between themselves.

The present analysis of the $N_2 + H_2$ jets rests upon Raman spectroscopy, which has proved successful for the quantitative study of supersonic expansions.[19,20] Accurate values of number density, and rotational and vibrational temperatures of molecular gases, are directly obtained from the Raman intensities, quantities that can be probed along and across the jet with a high spatial resolution without disturbing the flow. This methodology yields information on processes in the zone of silence like rotational−translational relaxation,[6,7] condensation onset, and cluster growth,[21,22] as well as precise data about the shock wave system.[23,24]

* Corresponding author. E-mail: a.ramos@iem.cfmac.csic.es.

10.1021/jp901700c CCC: $40.75
Published on Web 07/06/2009

TABLE 1: Four Expansions Analyzed in This Work[a]

sample	$X_0(N_2)$	Re_0	p_b (mbar)
N_2	1	7000	0.08
$2N_2 + H_2$	0.66(1)	6500	0.10
$N_2 + 2H_2$	0.34(1)	4400	0.13
H_2	0	3800	0.35

[a] Stagnation conditions: $p_0 = 1$ bar and $T_0 = 295$ K. Re_0 is the Reynolds number at the source, and p_b is the background pressure in the expansion chamber.

This paper is organized as follows. First, we describe the experimental setup and the methodology, based on Raman spectroscopy, as applied to $N_2 + H_2$ expansions. We then present the main results obtained in the zone of silence of the jets of these mixtures, including data of the pure N_2 and H_2 jets. We discuss next the rotational−translational relaxation processes and the separation of species along the jet axis, and we close the paper with some concluding remarks.

Experimental Section

Flow properties have been measured in continuous jets of pure N_2, H_2, and of their mixtures $N_2 + 2H_2$ and $2N_2 + H_2$, at stagnation pressure $p_0 = 1$ bar, and temperature $T_0 = 295$ K. The jets were generated expanding the gas through a cylindrical nozzle of diameter $D = 310$ μm, and internal length $L \approx 1.8$ mm, into a vacuum chamber specially devised for quantitative Raman spectroscopy measurements. Its vacuum system is based on a 1430 m^3/h Roots pump backed by a 70 m^3/h rotary pump.

The gas mixtures were prepared in the feed line from the pure gases, each flowing through a Bronkhorst High-Tech mass flow controller with an accuracy of 0.9 mmol/min, up to reaching a stagnation pressure of 1 bar in the mixture. The mole fractions of the mixtures were checked by means of their Raman spectra recorded under static conditions. The so measured stagnation mole fraction of nitrogen in the mixtures, $X_0(N_2)$, is shown in Table 1.

The zone of silence of the jets was probed at the lowest background pressure p_b the vacuum system could maintain in the expansion chamber, avoiding as far as possible the disturbances produced by the shock wave system. The background pressures, shown in Table 1, were measured to ± 0.01 mbar with a MKS Baratron pressure gauge. The dependence of p_b on the expanded gas is due to the different pumping speed of the vacuum system for H_2 and N_2.

A cw-Ar^+ laser was employed as excitation source at $\lambda = 514.5$ nm and 4 W output power, the scattered Raman radiation being collected at 90° with respect to the laser beam and the expansion axis. The scattered radiation was analyzed with an additive double monochromator, of 1 m focal length, equipped with a 2048 × 512 pixel CCD detector refrigerated by liquid nitrogen. The Raman spectra were recorded at ~0.3 cm^{-1} spectral resolution.

The excitation-collection optical system was kept fixed along the experiment, while the nozzle was positioned to reach the point of interest in the flow field. The pointing accuracy within the expansion flow field is ± 5 μm. Relative positions between two points are repeatable to ± 1 μm, which is the precision of the nozzle micropositioning actuators.

The spatial resolution of the experiment is determined by the volume in the jet actually seen by the detector of the spectrometer. This volume forms a cylinder-like region and is limited by the CCD readout system and by the laser beam waist.[19,23] The representative spatial resolution in this work was about $0.05D$ along the expansion axis (the diameter of the cylinder-like region); perpendicular to the expansion axis (the height of the cylinder-like region), along the laser beam, the spatial resolution ranges from $0.22D$ close to the nozzle up to $1.2D$ in the farthest points.

The number density and the rotational temperature of a tiny gas parcel in the expansion are measured by recording the Raman intensities scattered by that region. To a very good approximation the integrated Raman intensity I of the Q branch of a vibrational band is proportional to the number density n of the observed medium,

$$I_Q = Cn \tag{1}$$

C depends on exciting irradiance and wavelength, scattering geometry, and molecular polarizability derivative, factors which remain constant along the experiment. The factor C depends also on the local temperature of the gas; however, at temperatures below 300 K, this dependence is negligible for gases of low molecular weight ($w < 100$ amu).[25] The Q branch intensity recorded for N_2 is that of the vibrational band at 2331 cm^{-1}, whose $Q(J)$ components were not spectrally resolved; for H_2, the intensities of the fully resolved $Q(0)$, $Q(1)$, $Q(2)$, $Q(3)$ Raman lines at 4161.2, 4155.3, 4143.5, and 4125.9 cm^{-1}, respectively, were recorded. The estimated uncertainty of the measured absolute number densities depends on systematic as well as on random errors. The main source of systematic error arises from the elimination of constant C in eq 1 by comparing the intensity of the Raman signal of the expanding gas with that of a static sample of the same gas at known number density (reference density), both Raman spectra being recorded under identical optical conditions. Through the equation of state $p = knT$, the reference number density depends on pressure and temperature in the chamber. While the pressure is measured to better than 0.5% by means of the MKS-Baratron, the temperature is uncertain to ~5 K because of the heat released by the exciting laser beam (~4 W), which is unevenly distributed around the observed point. This may cause an estimated systematic error of ~2%. Random errors in the measured absolute number densities arise from the fluctuations of the Raman signals in eq 1, which in turn depend on the absolute number density, that is, on the distance to the nozzle. The total uncertainty (2σ = two standard deviations) estimated for systematic plus random errors is 5% close to the nozzle and 10% in the farthest section of the zone of silence.

The rotational temperatures are determined from the intensities I of the rotational lines, which are related to the populations P_J of the rotational levels J by[23,26]

$$I_{(v,J)\rightarrow(v',J')} = GP_J\overline{\langle v, J|\alpha|v', J'\rangle^2} \tag{2}$$

where α is the suitable component (trace or anisotropy) of the polarizability tensor for the employed scattering geometry; G is a constant factor that depends on exciting irradiance and wavelength. In this work, the vibrational levels for N_2 are $v = v' = 0$, with $J' = J + 2$, and for H_2, $v = 0$, $v' = 1$, and $J' = J$. In the present jets, the populations P_J of the rotational levels of each nuclear spin species within the ground vibrational state obey a Boltzmann distribution

$$P_J = (Z_R)^{-1} g_J(2J + 1)e^{-\beta(E_J - E_L)/T_R} \tag{3}$$

where Z_R is the rotational partition function, g_J is the spin statistical weight, $\beta = hc/k = 1.4388$ cm K, E_J is the rotational energy in cm^{-1}, E_L is the lowest rotational energy, and T_R is the rotational temperature. The rotational temperatures of N_2 have been determined by means of Boltzmann plots based on eq 3, which are nearly free from systematic errors. The standard deviation due to random errors in the rotational temperatures of N_2 is ~1%.

The hydrogen molecules are distributed into two noninterconverting spin species: ortho-H_2 (oH_2) and para-H_2 (pH_2), with fixed abundances 3:1. In the jet, they are characterized by different rotational temperatures, which are determined from the ratio of intensities of the $Q(2)$ to $Q(0)$ lines for pH_2 and of the $Q(3)$ to $Q(1)$ lines for oH_2. The rotational temperatures of pH_2 and oH_2 are also nearly free from systematic errors. The random errors depend on the abundance of H_2 in the $N_2 + H_2$ mixture, being higher the lower the fraction of H_2. The standard deviations (1σ) for pH_2 range from 1 to 3 K, and for oH_2, they range from 1.5 to 5 K depending on abundance and distance to the nozzle. The larger uncertainties of oH_2 rotational temperatures are attributed to the weak intensity of $Q(3)$ line compared with $Q(1)$.

Results

Axial Number Density. An overview of the measured absolute number densities of N_2 and H_2 along the axis of the studied expansions is shown in Figure 1, top, jointly with the density drop given by the isentropic model as an orientative reference; $\pm\sigma$ error bars (not shown) are smaller than the symbols employed. For clarity, the density values of the pure gas expansions are multiplied by 10, and those of the $2N_2 + H_2$ mixture are multiplied by 0.1. In the isentropic model, the axial number density is expressed as

$$n = n_0[1 + 0.5(\gamma - 1)M^2]^{-1/(\gamma-1)} \quad (4)$$

The Mach number M has been modeled here with the parameters given by Miller[3] for heat capacity ratio $\gamma = 7/5$, and a position of the sonic surface ($M = 1$) inside the nozzle at $z/D = -0.4$, which fits the isentropic densities to the experimental ones. This location of the sonic surface upstream the nozzle exit has been described for straight tube nozzles,[27] similar to the one used in this work. The value of the stagnation density in eq 4 is set to $n_0 = 24.553 \times 10^{24}$ m^{-3} for the pure expansions, as corresponding to their stagnation conditions $T_0 = 295$ K and $p_0 = 1$ bar; for the mixture expansions the stagnation densities of the two species are the corresponding to their partial pressures $p_0 = 1/3$ and 2/3 bar.

The differences in the decay of the number density along the various expansions are shown in detail in Figure 1, bottom, where the number densities of individual species N_2 or H_2, and of the total density of the $N_2 + 2H_2$ jet, are referred to that of the pure N_2 expansion. In the range $0.5 < z/D < 12$, the pure N_2 density decays according to the isentropic model prediction within ±4%, as shown by curve n(isentropic) of Figure 1, bottom. This is in good agreement with the estimated absolute error of the experimental number densities of 5 to 10%. The H_2 density in the pure jet decays clearly slower than the pure N_2 density, with values ~25% in excess at $z/D \approx 7$, the farthest point prior to the onset of the H_2 normal shock wave. This trend may be attributed to the increase of the effective γ of H_2, as a consequence of the fast freezing of the rotational degrees of freedom of ortho-H_2 and para-H_2 at ~180 K, as shown in Figure 2. The limit case would be that of the monatomic gases, with $\gamma = 5/3$. In both pure jets, the observed number densities tend asimptotically to $n \propto (z/D)^{-2}$, which is an intrinsic dependence of axisymmetric jets.

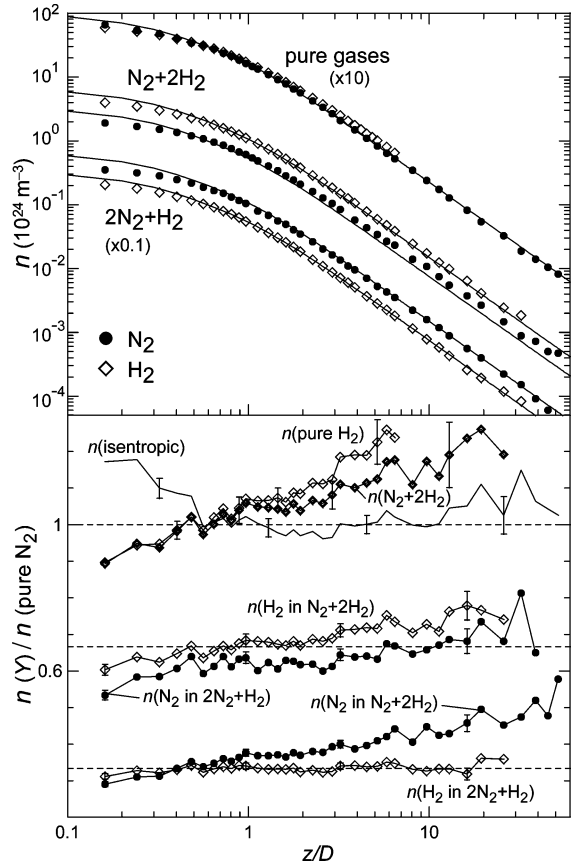

Figure 1. Top: Axial number densities n of N_2 and H_2 in the pure N_2 and pure H_2 expansions, and in the $N_2 + 2H_2$ and $2N_2 + H_2$ expansions. As a guide to the eye, solid lines indicate the isentropic number density for $\gamma = 7/5$ and sonic surface ($M = 1$) at $z/D = -0.4$. To avoid overlapping, there is a factor 10 for the pure gases data and a factor 0.1 for the $2N_2 + H_2$ jet. Bottom: Relative number density referred to that of the pure N_2 expansion; representative $\pm\sigma$ error bars are shown.

A detailed interpretation of the density decays in the $N_2 + 2H_2$ and $2N_2 + H_2$ expansions is not immediate because of the overlapping of two contributions; namely, (a) the change of the effective γ of the mixture along the axis, due to the different rotational cooling of N_2 and H_2, as discussed above for the pure H_2 jet, and (b) the on-axis enrichment of the heavy species, N_2, which will be discussed below.

The effect of the variation of γ in the mixture is shown by the relative total density of the $N_2 + 2H_2$ expansion (curve $n(N_2 + 2H_2)$ in Figure 1, bottom), whose decay is faster than that of the pure H_2 jet. In this mixture, the H_2 rotational cooling is more efficient (see Figure 2) than in the pure H_2 expansion, and as a consequence, $\gamma(H_2)$ is lower, yielding an effective γ closer to that of the pure N_2 expansion. The relative total density of the $2N_2 + H_2$ expansion (not shown in Figure 1) has the same trend, with an effective γ closer to γ(pure N_2) than $\gamma(N_2 + 2H_2)$, because of the lower H_2 content. On the other hand, the decay of the number density of N_2 in the two mixtures is in both cases slower than in the pure expansion, as shown in Figure 1, bottom, which indicates a N_2 enrichment on the axis.

Axial Temperatures. The rotational temperatures T_R of N_2 and H_2 along the axis of the expansions are shown in Figure 2.

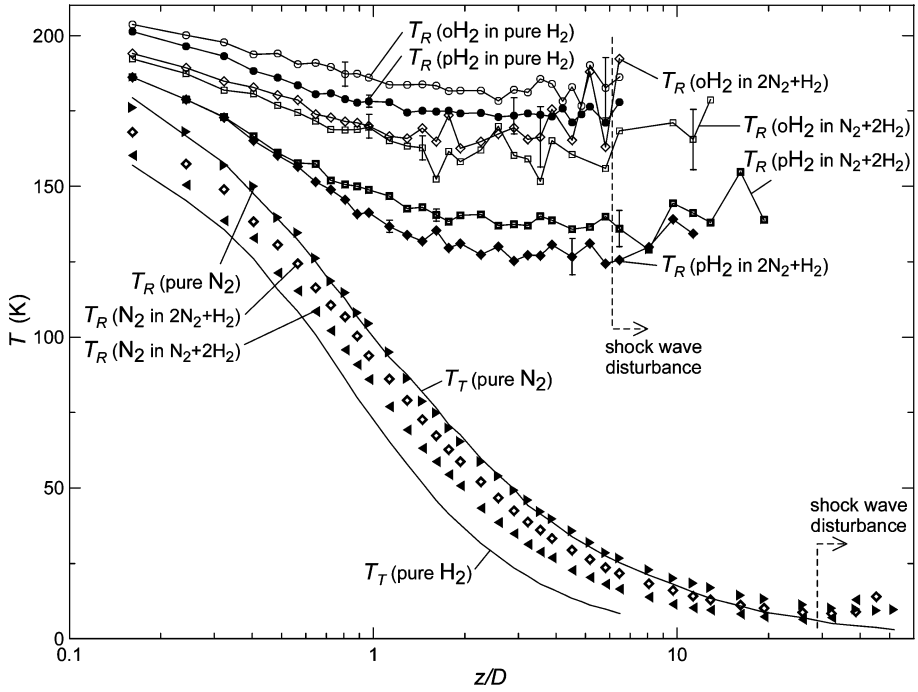

Figure 2. Rotational T_R and translational T_T temperatures of N_2 and H_2 along the jet axis. Representative $\pm\sigma$ error bars are shown for T_R of pH_2 and oH_2; error bars for T_R of N_2 are about the size of the symbols employed. For errors of T_T see the text.

Two different temperatures are measured for H_2, corresponding to the two species ortho, $T_R(oH_2)$, and para-hydrogen, $T_R(pH_2)$. Note that $T_R(H_2) > T_R(N_2)$ in all cases, and within the same expansion $T_R(oH_2) > T_R(pH_2)$, the larger the mole fraction $X_0(N_2)$, the greater the difference between the rotational temperatures of oH_2 and pH_2.

The further rise of the temperatures, at $z/D > 7$ for H_2 and $z/D > 28$ for N_2, is due to the disturbance by the normal shock wave, depicted as a vertical dashed line in Figure 2, whose location depends on the background pressure p_b in the expansion chamber. The position z_M of the normal shock wave is determined approximately by[28,29] $z_M = 0.67D\sqrt{p_0/p_b}$, the background pressure p_b varying in this work with the expanded gas as indicated in Table 1. In addition, the thermal shock wave profile depends on the species, and it has not the same onset nor width for H_2 and for N_2 because of their different efficiency in the rotation−translation energy transfer.

For the pure N_2 and pure H_2 expansions, the translational temperature T_T has been deduced from the experimental values of n, T_R, and the stagnation conditions, on the basis of the entropic invariance. The expressions for calculating T_T have been derived from the statistical definition of entropy,[6,7] taking $T_0 =$ 300 K. These translational temperatures are also shown in Figure 2. Random errors of T_T are ~2/3 of the sum of the random errors of number density and rotational temperature. Systematic errors of T_T depend on the uncertainty in the stagnation temperature and on the fulfillment of the isentropic invariance in the paraxial region of the jet. The weight of these two contributions can not be established at present. However, the good agreement of T_T and T_R at $z/D < 3$ in the expansion of pure N_2, and the smooth detachment of $T_T < T_R$ at $z/D > 3$ suggest that these systematic errors are small.

The equilibrium between rotational and translational temperatures in the expansion depends on the collision frequency and on the state-to-state cross sections σ for the different inelastic collision processes within the gas. The markedly different rotational cooling of N_2 and H_2 appears clearly in the T_R data of the pure expansions. This phenomenon has been exhaustively studied before.[5−7] The rotational degrees of freedom of pure hydrogen freeze very early in the present jets, with lowest pH_2 temperatures around 175 K, leading to an effective $\gamma > 7/5$ for H_2. On the contrary, the pure N_2 jet shows a quasi-equilibrium between translation and rotation, with very similar temperatures, until they diverge at $z/D > 7$. Downstream the collision frequency is not sufficient to maintain the rotation−translation equilibrium.

Rotational cooling of N_2 in the $N_2 + 2H_2$ and $2N_2 + H_2$ mixtures is more efficient than in the pure N_2 expansion, reaching lower temperatures for increasing mole fraction $X_0(H_2)$, as shown in Figure 2. A similar behavior has been observed in expansions of $N_2 + H_2$,[12] and of $N_2 + He$.[30] According to macroscopic fluid dynamics, like the isentropic model, a faster decay of the temperature is predicted as the value of γ is increased. As it has been discussed above, H_2 in the mixture makes the effective $\gamma > 7/5$, since its rotational degrees of freedom are partially frozen.

Microscopically the rotational cooling can be understood in terms of the inelastic collisions between the different partners, N_2, oH_2, pH_2, and their different efficiency of the rotational−translational energy transfer.[6] The present results imply that N_2:H_2 inelastic collisions are, on average, more efficient cooling processes for N_2 than N_2:N_2 self-collisions. According to the differences between the rotational temperatures of the species shown in Figure 2, the following relationship between inelastic rotational cross sections can be established: $\sigma(oH_2{:}H_2) < \sigma(pH_2{:}H_2) < \sigma(oH_2{:}N_2) < \sigma(pH_2{:}N_2) < \sigma(N_2{:}N_2) < \sigma(N_2{:}H_2)$, where (A:B) denotes the excitation/deexcitation of species A by collision with species B.

Radial Density and Temperature. For a more complete picture of the zone of silence of the expansion, measurements of densities and temperatures have been carried out along a perpendicular direction to the axis at $z/D = 1.9$. Figure 3 shows these data along the radial direction for the pure expansions.

Near the axis, the H_2 density drops with radial distance r faster than that of N_2 (Figure 3, top), but at $r/D > 3$, it tends toward a constant value, while the N_2 density continues decreasing at least up to $r/D = 6$, the farthest point measured.

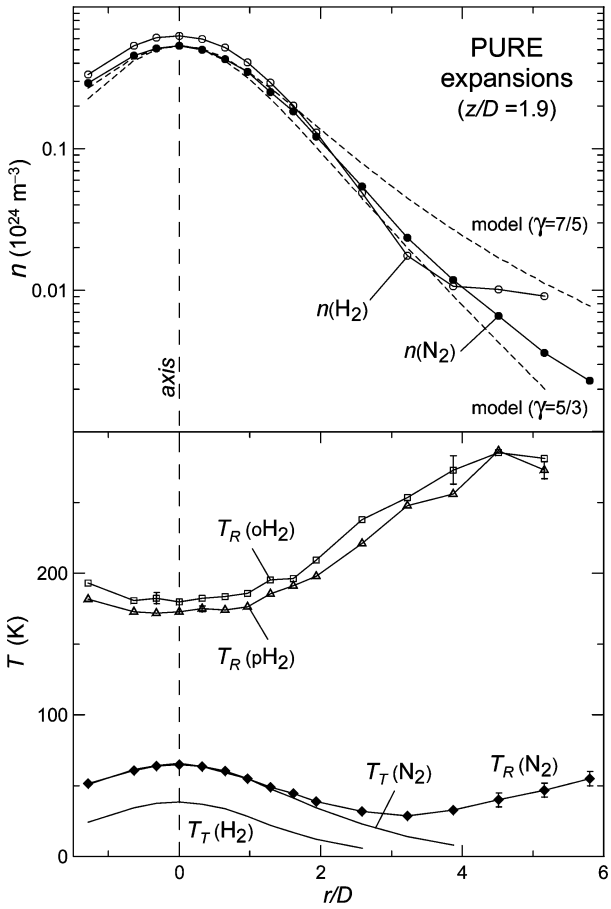

Figure 3. Number densities (top) and rotational T_R and translational T_T temperatures (bottom) along a radial direction at $z/D = 1.9$ of the pure expansions of N_2 and H_2. Representative $\pm\sigma$ error bars for T_R are shown. Dashed lines in top panel are the modeled radial density, eq 5, for the N_2 jet.

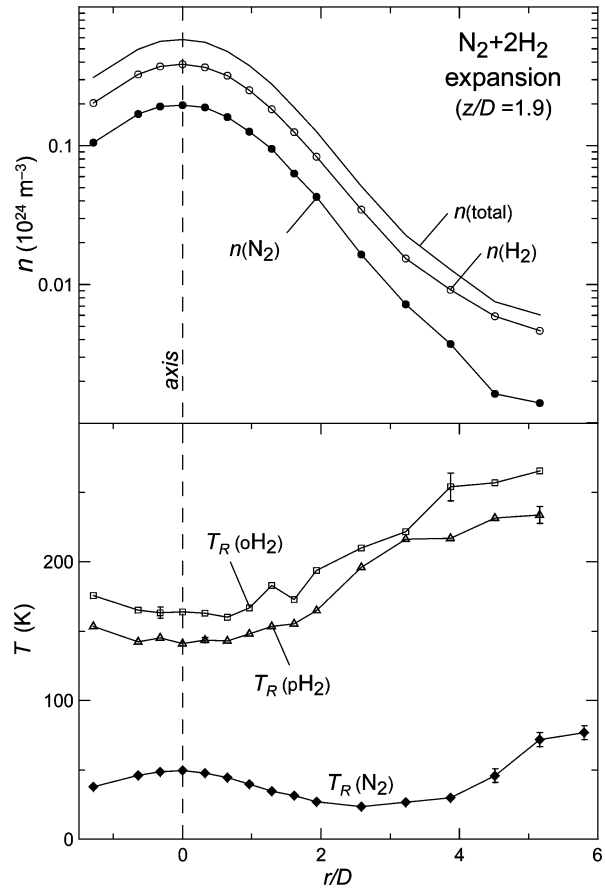

Figure 4. Number densities (top) and rotational temperatures (bottom) along the radial direction of the $N_2 + 2H_2$ expansion, at $z/D = 1.9$. Representative $\pm\sigma$ error bars for T_R are shown.

Since the ratio p_0/p_b is very different for pure N_2 and pure H_2 expansions (see Table 1), it may be expected that the pure H_2 normal shock wave and the associated barrel shock will be closer to the nozzle than in pure N_2 jet. Although the barrel shock is not yet completely formed at $z/D = 1.9$, its influence on the flow, and that of the nozzle rim, can affect the density drop along r.

The off-axis density according to the model of Ashkenas and Sherman[3,28] is also plotted in Figure 3, top, for the pure N_2 expansion. The density values of this model are given by

$$n(r, z) = n(0, z)\cos^2(\alpha)\cos^2(\phi\alpha) \qquad (5)$$

where $\alpha = \arctan(r/z)$, and the parameter ϕ was fitted to data calculated by the method-of-characteristics, with the approximation of an ideal initial condition of $M \cong 1$ in the plane of the nozzle exit; the values $\phi = 0.9451$ and 1.1508 were obtained for $\gamma = 7/5$ and 5/3, respectively.[28]

The modeled off-axis density for $\gamma = 7/5$ only agrees with the experimental data of the N_2 jet for $r/D < 1.5$; for $r/D > 1.5$, the measured density decreases faster than the predicted values, approaching the slope of the modeled density for $\gamma = 5/3$. Pure H_2 density shows an even greater deviation, since the present experimental data decay faster than the model prediction for $\gamma = 5/3$.

The rotational temperatures along r have a very different trend for both gases, as can be seen in Figure 3. For N_2, the gas gets colder for increasing distances from the axis up to $r/D \sim 3$, and then it heats up, while the H_2 rotational temperature rises from its minimum, which is located on the axis. This indicates that the gas is perturbed by the thermal barrel shock at a shorter distance to the axis than by the density barrel shock. Furthermore, the thermal barrel shock is broader for H_2 than for N_2, almost reaching the axis in the pure H_2 jet. A thorough analysis of the shock waves created on expansions of pure N_2, pure H_2, and $N_2 + 2H_2$ will be the subject of a forthcoming paper.

The translational temperatures T_T are also shown in Figure 3. They have been calculated assuming constant entropy along the radial direction r, in the same way as the T_T was calculated along the axis. The isentropic character within the zone of silence is commonly used and accepted in free jet works. Taking into account that flow lines around the axis have the same source, we can assume the same constant entropy along r, except when the flow has been perturbed by the barrel shock or the nozzle walls. The calculated T_T is in good agreement with the T_R of N_2 for $-1.5 < r/D < 1.5$, an indication of the isentropic character of the expansion core, and of its rotation−translation quasi-equilibrium. The translational temperatures calculated for H_2 show a similar trend to those of N_2, with lower values consistent with the axial data (see Figure 2).

The number densities and the rotational temperatures along the radial direction of the $N_2 + 2H_2$ expansion are plotted in Figure 4. Densities decrease monotonically, with no evidence of a density rise as in the pure H_2 jet shown in Figure 3. The rotational temperatures of both gases have a similar behavior to those of the pure expansions, though scaled to lower values at the axis, in agreement with the data shown in Figure 2.

Diffusive Separation. One of the phenomena shown by the present measurements is the effect of the diffusive separation of species in the expansion of a mixture, which results in a concentration of the heavier species in the jet core. Early measurements of this separation in free expansions of $N_2 + H_2$ mixtures[9] were explained as a consequence of the interaction of the supersonic flow with the skimmer or sampling tube. However, nonintrusive techniques as electron beam fluorescence confirmed the separation effect in rarefied He−Ar flows.[11] The gasdynamic theory of diffusive separation of mixtures in a free jet developed by Sherman[10] combines the continuum flow conservation equations for a two-component mixture with the binary diffusion equation based on the Chapman−Enskog theory. It expresses the quantities f's of the flow in terms of inverse powers of the stagnation Reynolds number Re_0,

$$f = f^{(0)} + f^{(1)}/\mathrm{Re}_0 + f^{(2)}/\mathrm{Re}_0^2 + \cdots \qquad (6)$$

where $Re_0 = \rho_0 a_0 D/\mu_0$, ρ_0 is the mass density, a_0 is the sonic velocity, D is the nozzle diameter, and μ_0 is the dynamic viscosity. In the zero-order approximation of eq 6, the flow is isentropic, and the mixture remains homogeneous. The first-order approximation, applied to the central streamline of an axisymmetric flow, gives the mole fraction X of the heavy component along the axis as a function of the Mach number and of some parameters which depend on the mixture.[11]

This theory is in good agreement with the experimental enrichment of the heavy component along the jet axis of He + Ar[11] and $CO_2 + H_2$[13] expansions, over the ranges $100 < Re_0 < 10000$ and $100 < Re_0 < 3000$, respectively. Most of the reported enrichment takes place over a distance $z/D < 10$ for molecular mixtures, being faster for mixtures of monatomic gases. Furthermore, a very small separation was observed for $Re_0 > 5000$ in the He + Ar expansions,[11] as predicted by the theory.

The expansions of the mixtures analyzed in the present work have Reynolds numbers at the source $Re_0 \approx 4400$ and $Re_0 \approx 6500$, as shown in Table 1, calculated with the mixture viscosity μ_0 derived from Wilke's formula.[31] A small enrichment of N_2 along the jet axis is expected with such high values of Re_0. The measured mole fraction of N_2 normalized to the first point, $\xi(N_2)$, is shown in Figure 5a. In spite of the data dispersion, a clear trend of increasing enrichment is observed. A fast growth of $\xi(N_2)$ occurs at the beginning of the expansion, where the pressure gradient is larger and consequently the diffusive effect is stronger. For $z/D > 1$, $\xi(N_2)$ increases slower, up to a maximum value of about 14% and 6% for the $N_2 + 2H_2$ and $2N_2 + H_2$ mixtures, respectively. The lower measured enrichment corresponds to the expansion with greater Re_0, in agreement with the theory.[10,11]

The predictions from Sherman's theory are shown in Figure 5a as continuous lines, normalized to their values at the first experimental point. Their calculation is based on Miller's Mach number model[3] with the sonic position ($M = 1$) at $z/D = -0.4$. Probably, this model is not accurate within the nozzle, nor in the points very close to it. The inaccuracy of the Mach number near the nozzle yields an uncertainty of about 10% in the calculated enrichment for $z/D > 1$.[10] The present experimental values of N_2 enrichment are higher than the predicted ones (see Figure 5a), as in other works with such high Re_0,[13] in qualitative agreement with the theory.

The relative N_2 mole fraction along a direction perpendicular to the axis of the $N_2 + 2H_2$ jet, also normalized to the first axial point, is shown in Figure 5b. These measurements correspond to the section at $z/D = 1.9$, shown in Figure 4, with the presence of a weak barrel shock, far away from the axis. It can be seen that $\xi(N_2)$ decreases off the axis from $r/D \approx 2$ on. This can be explained by the radial diffusion due to the pressure gradient, which causes the enrichment of N_2 on the axis and its corresponding deficit off the axis.[11]

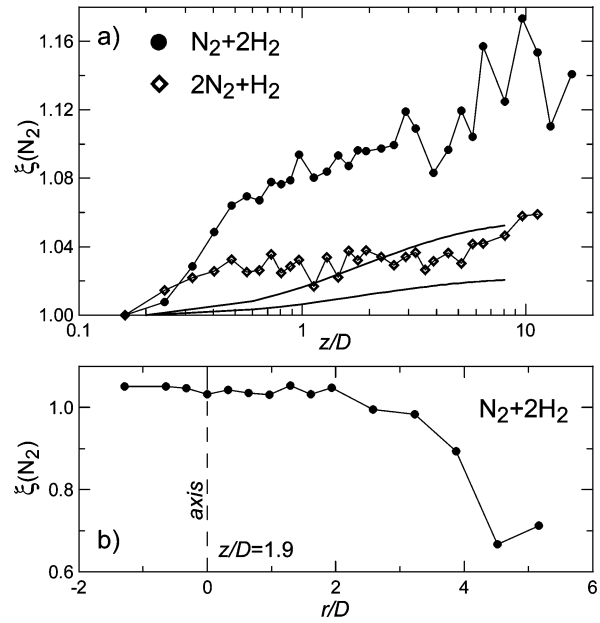

Figure 5. (a) Relative mole fraction of nitrogen $\xi(N_2)$ along the jet axis. Continuous lines are the expected theoretical values. (b) $\xi(N_2)$ along the radial direction of the $N_2 + 2H_2$ expansion, at $z/D = 1.9$.

Summary and Conclusions

We have presented an extensive data set of number densities and rotational temperatures of H_2 and N_2 in the zone of silence of continuous jets of two mixtures, $N_2 + 2H_2$ and $2N_2 + H_2$, as well as in jets of the pure gases.

The measured number density along the axis of the pure N_2 jet decays as predicted by the isentropic model for $\gamma = 7/5$ within 4%. For all of the other jets, the measured total density tends to deviate from the isentropic prediction. In the expansions of the mixtures, a slower density decay is observed for increasing H_2 molar fraction, with the slowest density drop corresponding to the pure H_2 jet. This effect can be related to an increasing effective γ of the expanded gas as the H_2 rotational degrees of freedom become frozen. The asymptotic trend $n \propto (z/D)^{-2}$, which is intrinsic to axisymmetric jets, is observed for $z/D > 10$ in all cases.

The measured rotational temperatures T_R of N_2 and of the two spin species, ortho-H_2 and para-H_2, show a very different behavior in the rotation−translation energy transfer. A freezing of the H_2 rotational degrees of freedom is observed, more pronounced in the pure H_2 expansion, where the rotational temperatures freeze at ~180 K. In the expansions of the mixtures, the rotational cooling of N_2 and H_2 is more efficient than in the pure jets. Nitrogen T_R becomes lower for increasing H_2 mole fraction, and hydrogen T_R gets lower in average for larger N_2 content; furthermore, a larger split between $T_R(oH_2)$ and $T_R(pH_2)$ is observed for increasing N_2 mole fraction. Microscopically, the behavior of the rotational temperatures depends on the energy transfer efficiency in the inelastic collisions between the different species. A relationship between rotational cross sections of the different inelastic collision processes is inferred from the present measurements.

On-axis enrichment of the heavier species has been measured in the expansions of the mixtures. The predictions from a gasdynamic theory of diffusive separation[10] agree qualitatively with the present measurements. In the expansion with lower Reynolds number at the source, $N_2 + 2H_2$, an enrichment of N_2 of about 14% is observed for $z/D > 8$.

Radial measurements of number density and rotational temperature are also presented, providing an off-axis view of the nonequilibrium between rotational degrees of freedom, and of the N_2 on-axis enrichment in the mixtures. For the pure expansions of N_2 and H_2, these data do not support the off-axis density model by Ashkenas and Sherman.[28]

In conclusion, we have investigated quantitatively the main aspects of the gasdynamics and of the nonequilibrium phenomena in the zone of silence of supersonic expansions of $N_2 + H_2$ mixtures. From the experimental point of view, we confirm by means of the present results the power of Raman spectroscopy for the quantitative study of these rarified gas systems, yielding accurate data with a high spatial resolution. The experimental data set reported in this work provides valuable material for testing the kinetic theory of gas mixtures and the related computational Monte Carlo codes under marked nonequilibrium conditions. Also, it will serve as a useful starting point for future quantitative studies on inellastic collisions between N_2 and H_2 molecules. In a forthcoming paper, the study of the present expansions will be extended with experimental data of number density and rotational temperatures across the normal and the barrel shocks.

Acknowledgment. A. Ramos acknowledges CSIC for an I3P grant. This work has been supported by the Spanish Ministerio de Educación y Ciencia, research Project No. FIS2004-02576 and Project No. FIS2007-61430, and by the Comunidad de Madrid, Project No. S-0505/ESP/0237(ASTROCAM).

Supporting Information Available: Supporting tables are available with the experimental data of the number densities and the rotational temperatures plotted in Figure 1, top, Figure 2, Figure 3, and Figure 4. The axial isentropic density used as a reference in Figure 1, and the calculated translational temperatures of the pure expansions, are also included. This material is available free of charge via the Internet at http://pubs.acs.org.

References and Notes

(1) Giovangigli, V. *Multicomponent flow modeling*; Birkhauser: Boston, 1999.
(2) Zhdanov, V. M.; Tirskiy, G. A. *J. Appl. Math. Mech.* **2007**, *71*, 718–736.
(3) Miller, D. R. Free jet sources. In *Atomic and Molecular Beam Methods*, Vol. I.; Scoles, G., Ed.; Oxford University Press: New York, 1988.
(4) Sharafutdinov, R. G.; Belikov, A. E.; Strekalov, M. L.; Storozhev, A. V. *Chem. Phys.* **1996**, *207*, 193–201.
(5) Ramos, A.; Tejeda, G.; Fernández, J. M.; Montero, S. *Phys. Rev. A* **2002**, *66*, 022702.
(6) Montero, S.; Thibault, F.; Tejeda, G.; Fernández, J. M. *J. Chem. Phys.* **2006**, *125*, 124301.
(7) Fonfría, P.; Ramos, A.; Thibault, F.; Tejeda, G.; Fernández, J. M.; Montero, S. *J. Chem. Phys.* **2007**, *127*, 134305.
(8) Wang-Chang, C. S.; Uhlenbeck, G. E.; deBoer, J. The heat conductivity and viscosity of polyatomic gases. In *Studies in Statistical Mechanics*, Vol. 2; deBoer, J., Uhlenbeck, G. E., Eds.; North-Holland: Amsterdam, 1964.
(9) Reis, V. H.; Fenn, J. B. *J. Chem. Phys.* **1963**, *39*, 3240–3250.
(10) Sherman, F. S. *Phys. Fluids* **1965**, *8*, 773–779.
(11) Rothe, D. E. *Phys. Fluids* **1966**, *9*, 1643–1658.
(12) Bochkarev, A. A.; Kosinov, V. A.; Prikhod'ko, V. G.; Rebrov, A. K. *J. Appl. Mech. Tech. Phys.* **1972**, *13*, 804–808.
(13) McCay, T. D.; Price, L. L. *Phys. Fluids* **1983**, *26*, 2115–2119.
(14) de la Mora, J. F.; Rosell-Llompart, J. *J. Chem. Phys.* **1989**, *91*, 2603–2615.
(15) Raghuraman, P.; Davidovits, P. *Phys. Fluids* **1978**, *21*, 1485–1489.
(16) Piseri, P.; Tafreshi, H. V.; Milani, P. *Curr. Opin. Solid State Mater. Sci.* **2004**, *8*, 195–202.
(17) Mori, H.; Dankert, C. Spectroscopy of $H_2^- + N_2^-$ mixture in rarefied flows. In *23rd Rarefied Gas Dynamics, Vol. 663*; Ketsdever, A. D., Muntz, E. P., Eds.; AIP Conference Proceedings, 2003.
(18) Boyd, I. D.; VanGilder, D. B.; Beiting, E. J. *AIAA J.* **1996**, *34*, 2320–2326.
(19) Montero, S.; Maté, B.; Tejeda, G.; Fernández, J. M.; Ramos, A. Raman studies of free jet expansions (diagnostics and mapping). In *Atomic and Molecular Beams. The State of the Art 2000*; Campargue, R., Ed.; Springer-Verlag: New York, 2001.
(20) Maté, B.; Graur, I. A.; Elizarova, T. G.; Chirokov, I.; Tejeda, G.; Fernández, J. M.; Montero, S. *J. Fluid Mech.* **2001**, *426*, 177–197.
(21) Tejeda, G.; Fernández, J. M.; Montero, S.; Blume, D.; Toennies, J. P. *Phys. Rev. Lett.* **2004**, *92*, 223401.
(22) Ramos, A.; Fernández, J. M.; Tejeda, G.; Montero, S. *Phys. Rev. A* **2005**, *72*, 053204.
(23) Ramos, A.; Maté, B.; Tejeda, G.; Fernández, J. M.; Montero, S. *Phys. Rev. E* **2000**, *62*, 4940–4945.
(24) Graur, I. A.; Elizarova, T. G.; Ramos, A.; Tejeda, G.; Fernández, J. M.; Montero, S. *J. Fluid Mech.* **2004**, *504*, 239–270.
(25) Schrötter, H. W.; Klöckner, H. W. Raman scattering cross sections in gases and liquids. In *Raman spectroscopy of gases and liquids*; Weber, A., Ed.; Springer-Verlag: Berlin, 1979.
(26) Tejeda, G.; Maté, B.; Fernández-Sánchez, J. M.; Montero, S. *Phys. Rev. Lett.* **1996**, *76*, 34–37.
(27) Murphy, H. R.; Miller, D. R. *J. Phys. Chem.* **1984**, *88*, 4474–4478.
(28) Ashkenas, H.; Sherman, F. S. The structure and utilization of supersonic free jets in low density wind tunnels. In *4th Rarefied Gas Dynamics, Vol. II*; de Leeuw, J. H., Ed.; Academic Press: New York, 1966.
(29) Young, W. S. *Phys. Fluids* **1975**, *18*, 1421–1425.
(30) Maté, B.; Thibault, F.; Ramos, A.; Tejeda, G.; Fernández, J. M.; Montero, S. *J. Chem. Phys.* **2003**, *118*, 4477–4486.
(31) Wilke, C. R. *J. Chem. Phys.* **1950**, *18*, 517–519.

JP901700C